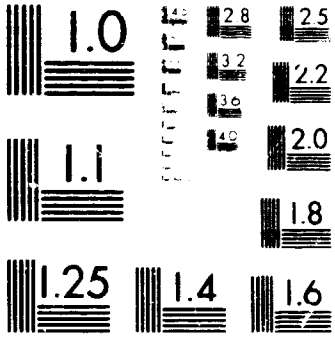

NASA
Technical Memorandum 78729

AVRADCOM
Technical Report 78-34

Analysis of Stability Contributions of High Dihedral V-Tails

Carl E. Freeman and William T. Yeager, Jr.
Structures Laboratory, AVRADCOM Research and Technology Laboratories
Langley Research Center
Hampton, Virginia

National Aeronautics
and Space Administration

**Scientific and Technical
Information Office**

1978

SUMMARY

An investigation was undertaken to determine the effectiveness of four analytical methods (empirical, modified empirical, vortex-lattice, and an inviscid, three-dimensional, potential-flow, wing-body program) to estimate the lateral and longitudinal static stability characteristics of an isolated V-tail wind-tunnel model. The experimental tests were conducted in the Langley V/STOL tunnel at a Mach number of 0.18. Angle-of-attack data were obtained from -12° to 8° at 0° sideslip. Sideslip sweeps from -5° to 10° were made at angles of attack of 4°, 0°, and -4°. The V-tail dihedral angles were 45°, 50°, 55°, and 60°. Of the methods used, a combination of the modified empirical and vortex-lattice methods correlated with the experimental results best except for predicting static directional stability contributions at high dihedral angles. The inviscid, three-dimensional, potential-flow, wing-body program correlated better at high dihedral angles.

INTRODUCTION

Conventionally powered, single-rotor helicopters have experienced directional control problems while operating in low-velocity, left-rear-quartering winds in ground effect and during low-speed sideward flight in ground effect (refs. 1 and 2). Investigations have been conducted to determine the source of these directional control problems and possible means of alleviating them (refs. 3 to 5). Reference 4 shows that a V-type empennage can present significant advantages over conventional horizontal-vertical control surfaces for helicopter directional control at low speeds. The principal advantages are smaller adverse fin forces and increased tail-rotor efficiency.

An important aspect of designing a V-type empennage is the ability to predict its aerodynamic characteristics in terms of longitudinal and directional static stability. Previous work in this area, such as references 6 and 7, used a simplified method to predict the aerodynamic characteristics of lifting surfaces with increasing dihedral angle. The accuracy of this method was found to be deficient for V-tails with dihedral angles greater than 40°.

An investigation was conducted to evaluate the effectiveness of the simplified method of references 6 and 7 and of more sophisticated vortex-lattice and inviscid-flow paneling methods in determining the effects of dihedral on the static stability characteristics of an isolated V-tail. Wind-tunnel tests of a helicopter V-type empennage were conducted and the results were used as a basis for comparison with the analytical methods.

SYMBOLS

Units used for physical quantities defined in this paper are given in the International System of Units (SI) and parenthetically in U.S. Customary Units.

Measurements and calculations were made in U.S. Customary Units. Conversion factors are presented in reference 8. The positive directions of forces are shown in figure 1.

c_l section lift coefficient

C_L total lift coefficient (stability axis), $F_L/q_\infty S$

C_{L_α} lift-curve slope, $dC_L/d\alpha$, per deg

C_Y side-force coefficient (body axis), $F_Y/q_\infty S$

C_{Y_β} slope of side-force curve, $dC_Y/d\beta$, per deg

F_L lift force, N (lbf)

F_Y side force, N (lbf)

i_v incidence angle, deg

K correction factor for C_{Y_β} (ref. 6)

q_∞ dynamic pressure, Pa (lbf/ft^2)

S total V-tail area, 0.244 m^2 (2.625 ft^2)

α angle of attack, deg

β angle of sideslip, deg

Γ dihedral angle, deg

Subscript:

N normal to surface

APPARATUS AND EXPERIMENTAL TEST PROCEDURES

The experimental data presented in this report were obtained on the tail-alone configuration shown in figure 2. Dimensions and geometric data are given in figure 1. The model was mounted on a six-component strain-gage balance. A bluff forebody was attached to the strut to close off the tail cone. Transition grit was applied to the tail surfaces.

The tests were conducted in the Langley V/STOL tunnel, which is an atmospheric, closed-circuit wind tunnel. The test section measures 4.2 m (14.50 ft) by 6.63 m (21.75 ft). Data were obtained at a free-stream dynamic pressure of 2.30 kPa (48 lbf/ft^2), which corresponds to a Mach number of 0.18. Model angle-of-attack sweeps were made from -12° to 8° at $\beta = 0^\circ$. Sideslip sweeps were made from -5° to 10° at $\alpha = 4^\circ$, 0°, and -4°. Pitch measurements were made using an internal pitch accelerometer. Yaw angle was measured externally.

The strut support was held parallel to the test-section center line for the sideslip sweeps to minimize strut interference on the model. No wall corrections were made.

The incidence angle and dihedral angle of each tail surface of the model could be independently varied. For this investigation the incidence angle of both tail surfaces was fixed at 5°, as shown in figure 1. Four dihedral angles were tested: 45°, 50°, 55°, and 60°. The experimental data presented in this report are the result of subtracting tail-cone data from data for the tail cone plus the tail surfaces to obtain data for the tail surfaces.

ANALYTICAL METHODS

Experimental data were compared with results from four analytical methods to determine the ability of these methods to predict the effects of dihedral angle on the static stability characteristics of an isolated V-tail. The four analytical methods used were (1) the simplified analysis of reference 6, the Purser-Campbell method; (2) a modified version of the Purser-Campbell method; (3) the vortex-lattice method of reference 9; and (4) the inviscid, three-dimensional (3-D), potential-flow program of reference 10.

The assumptions made by the Purser-Campbell method are basically there is no interference between the tail surfaces with dihedral, and lift and side force are simple geometric functions of dihedral; and the lift-curve slope normal to the tail surface with dihedral is equal to the lift-curve slope of the tail surfaces at 0° dihedral. These assumptions simplify the expressions for the tail contribution to longitudinal and directional stability to

$$C_{L_\alpha} = \left(C_{L_\alpha}\right)_N \cos^2 \Gamma \tag{1}$$

$$C_{Y_\beta} = -K\left(C_{L_\alpha}\right)_N \sin^2 \Gamma \tag{2}$$

The modified Purser-Campbell method makes use of equations (1) and (2) and uses the same value of K used in the Purser-Campbell method, but $\left(C_{L_\alpha}\right)_N$ is obtained by using the vortex-lattice method of reference 9.

The vortex-lattice method of reference 9 used 6 chordwise and 10 spanwise rows of panels to model the V-tail. The left surface of the V-tail was modeled from the dihedral hinge line to the tip; the right surface was modeled from the dihedral hinge line to the midpoint of the tail-rotor gearbox fairing. The spanwise loads were summed from the point 6.25 cm (2.46 in.) from the dihedral hinge line to the outboard end of each respective surface. This inboard point represents the juncture of the tail surfaces and the tail cone. The vortex-lattice method has a potential deficiency in its ability to model this V-tail configuration. This potential deficiency may arise because the experimental V-tail model uses a relatively thick (15 percent) airfoil section, whereas the vortex-lattice method is based on thin-airfoil assumptions.

The inviscid, three-dimensional, potential-flow program utilizes source panels to represent nonlifting surfaces and doublet panels on source panels to represent lifting surfaces. Neumann boundary conditions of tangential flow are assumed. The V-tail configuration as modeled for this program is shown in figure 3. Discrete components were used for the modeling to allow for easier alterations in the paneling scheme when dihedral angle was changed. A total of 860 panels was used to model the lifting surface and three chordwise panels behind each lifting surface were used to model the wake. A cosine distribution of panels was used on the lifting surfaces. Doublet panels alone were extended 2.54 cm (1.0 in.) into the body, and loads were summed for the tail surfaces only.

RESULTS AND DISCUSSION

Experimental data from the wind-tunnel test of the isolated V-tail are presented in figures 4 to 7. In figure 4 longitudinal aerodynamic data are presented in the form of C_L as a function of α for dihedral angles of 45°, 50°, 55°, and 60°. As expected, the lift-curve slope decreases with increasing dihedral because of the reduction in projected horizontal surface area. Also, as dihedral angle increases, the lift curves become nonlinear over the angle-of-attack range tested.

In figure 5 longitudinal aerodynamic data are presented for three tail configurations: right and left surfaces together at $\Gamma = 55°$, left surface only at $\Gamma = 55°$, and right surface only at $\Gamma = 55°$. Also shown in figure 5 (as the dashed line) is the sum of the lift coefficients of the individual surfaces. This figure indicates that a beneficial interference occurs between the two tail surfaces, since C_{L_α} of the total configuration is greater than that of the sum of the individual tail surfaces. In addition, the interference between the tail surfaces appears to be nonlinear with changes in angle of attack.

Figures 6 and 7 present lateral stability data in the form of C_Y as a function of β. In figure 6 the data are presented for three angles of attack at each of the four dihedral angles tested. For the three values of angle of attack, the value of C_{Y_β} became more negative as dihedral angle was increased. In contrast to the lift curves, the side-force curves became more linear with increasing dihedral angle over the range of sideslip angles tested.

In figure 7 are presented the lateral stability data for three tail configurations: right and left surfaces together at $\Gamma = 55°$, left surface only at $\Gamma = 55°$, and right surface only at $\Gamma = 55°$. Also shown is the sum of the side-force coefficients of the individual surfaces (dashed line). In contrast to the longitudinal aerodynamic data, a nonbeneficial interference occurred between the two tail surfaces, since the value of C_{Y_β} is less negative for the total configuration than for the sum of the individual tail surfaces.

The primary results of this investigation are summarized in figure 8 as a comparison of calculated values of C_{L_α} and $-C_{Y_\beta}$ with values of these derivatives determined from the wind-tunnel data shown in figures 4 and 6(b). The values of C_{L_α} were obtained at $\beta = 0^\circ$ between $\alpha = -5^\circ$ and 5°, and the values of $-C_{Y_\beta}$ were obtained at $\alpha = 0^\circ$ between $\beta = -5^\circ$ and 5°. The four analytical methods were described earlier.

As shown in figure 8, the best correlations with the experimental values of C_{L_α} were obtained with the modified Purser-Campbell and vortex-lattice methods. The other two methods gave values of C_{L_α} higher than the measured values; the least satisfactory correlation was obtained with the Purser-Campbell method.

Figure 8 also shows the variation of $-C_{Y_\beta}$ with increasing dihedral angle. Two of the distributions of $-C_{Y_\beta}$ (Purser-Campbell and modified Purser-Campbell methods) were predicted by use of equation (2). As previously shown in equation (2), the value of $-C_{Y_\beta}$ predicted is dependent on K and $\left(C_{L_\alpha}\right)_N$ for any given dihedral angle. The value of K (0.65) was determined from figure 2 of reference 6, and $\left(C_{L_\alpha}\right)_N$ was determined as previously described. For the Purser-Campbell method, the results do not correlate well with the experimental data; for the modified Purser-Campbell method, the correlation with the experimental data is much better. However, neither of the two methods using equation (2) predicts the reduction in the slope of $-C_{Y_\beta}$ versus Γ shown by the experimental data at the higher dihedral angles. Both the vortex-lattice and 3-D potential flow methods correlate the experimental data better, particularly in predicting the reduction in $-C_{Y_\beta}$ as Γ approaches the value where the two surfaces would converge into one, as described in reference 6. This reduction in $-C_{Y_\beta}$ at the higher dihedral angles is due to increased interference between the two V-tail surfaces, which is more accurately predicted by these more sophisticated methods. Changing the value of K or $\left(C_{L_\alpha}\right)_N$ in equation (2) will still not enable the modified Purser-Campbell method to accurately predict the reduction in $-C_{Y_\beta}$ indicated by the experimental results, since the results from equation (2) will still follow a sine-squared distribution of dihedral angle.

CONCLUDING REMARKS

An investigation was undertaken to determine the ability of four analytical methods to accurately predict the lateral and longitudinal static stability characteristics of an isolated V-tail model. It was determined from this investigation that a simplified prediction method used in conjunction with a vortex-lattice method gave adequate results for the longitudinal static stability characteristics at moderate dihedral angles. This combination of methods was deficient in the prediction of tail contribution to static directional stability at high dihedral angles. A more sophisticated method based on an inviscid, three-dimensional, wing-body, potential-flow program sufficiently predicted the tail contributions to static directional stability at the higher dihedral angles. However, this method was deficient in the prediction of longitudinal static stability characteristics.

Langley Research Center
National Aeronautics and Space Administration
Hampton, VA 23665
July 20, 1978

REFERENCES

1. Connor, William J.: The Huey Cobra in Vietnam. 1968 Report to the Aerospace Profession, Tech. Rev., vol. 9, no. 2, Soc. Exp. Test Pilots, 1968, pp. 25-32.

2. Lynn, R. R.; Robinson, F. D.; Batra, N. N.; and Duhon, J. M.: Tail Rotor Design. Pt. I: Aerodynamics. J. American Helicopter Soc., vol. 15, no. 4, Oct. 1970, pp. 2-15.

3. Huston, Robert J.; and Morris, Charles E. K., Jr.: A Wind-Tunnel Investigation of Helicopter Directional Control in Rearward Flight in Ground Effect. NASA TN D-6118, 1971.

4. Yeager, William T., Jr.; Young, Warren H., Jr.; and Mantay, Wayne R.: A Wind-Tunnel Investigation of Parameters Affecting Helicopter Directional Control at Low Speeds in Ground Effect. NASA TN D-7694, 1974.

5. Wiesner, Wayne; and Kohler, Gary: Tail Rotor Design Guide. USAAMRDL Tech. Rep. 73-99, U.S. Army, Jan. 1974. (Available from DDC as AD 775 391.)

6. Purser, Paul E.; and Campbell, John P.: Experimental Verification of a Simplified Vee-Tail Theory and Analysis of Available Data on Complete Models With Vee Tails. NACA Rep. 823, 1945. (Supersedes NACA ACR L5A03.)

7. Schade, Robert O.: Effect of Geometric Dihedral on the Aerodynamic Characteristics of Two Isolated Vee-Tail Surfaces. NACA TN 1369, 1947.

8. Mechtly, E. A.: The International System of Units - Physical Constants and Conversion Factors (Second Revision). NASA SP-7012, 1973.

9. Tulinius, J.: Unified Subsonic, Transonic, and Supersonic NAR Vortex Lattice. TFD-72-523, Los Angeles Div., North American Rockwell, Apr. 27, 1972.

10. Hess, John L.: Calculation of Potential Flow About Arbitrary Three-Dimensional Lifting Bodies. Rep. No. MDC J5679-01 (Contract N00019-71-C-0524), McDonnell Douglas Corp., Oct. 1972. (Available from DDC as AD 755 480.)

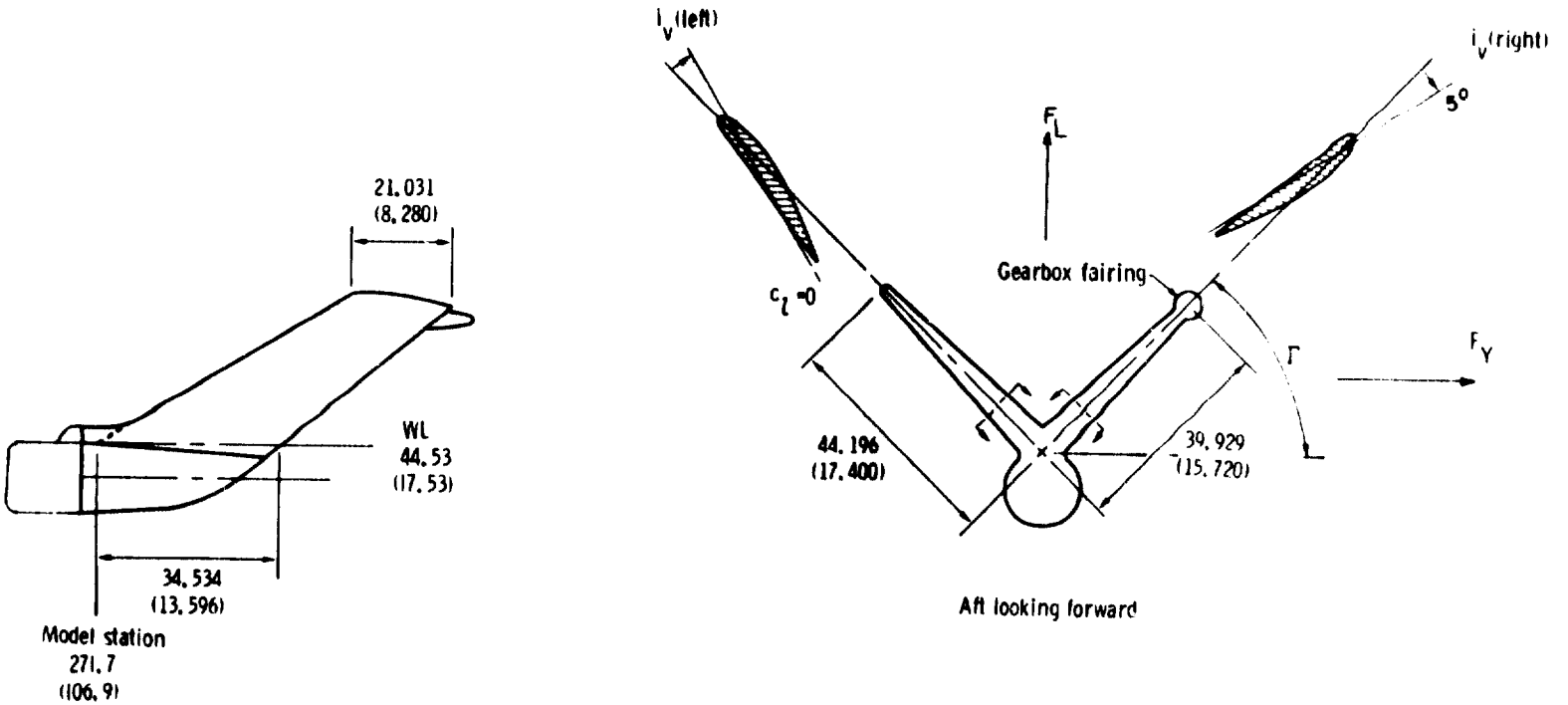

Figure 1.- V-tail geometry.. Dimensions are given in cm (in.).

L-76-4116

Figure 2.- V-tail without fuselage.

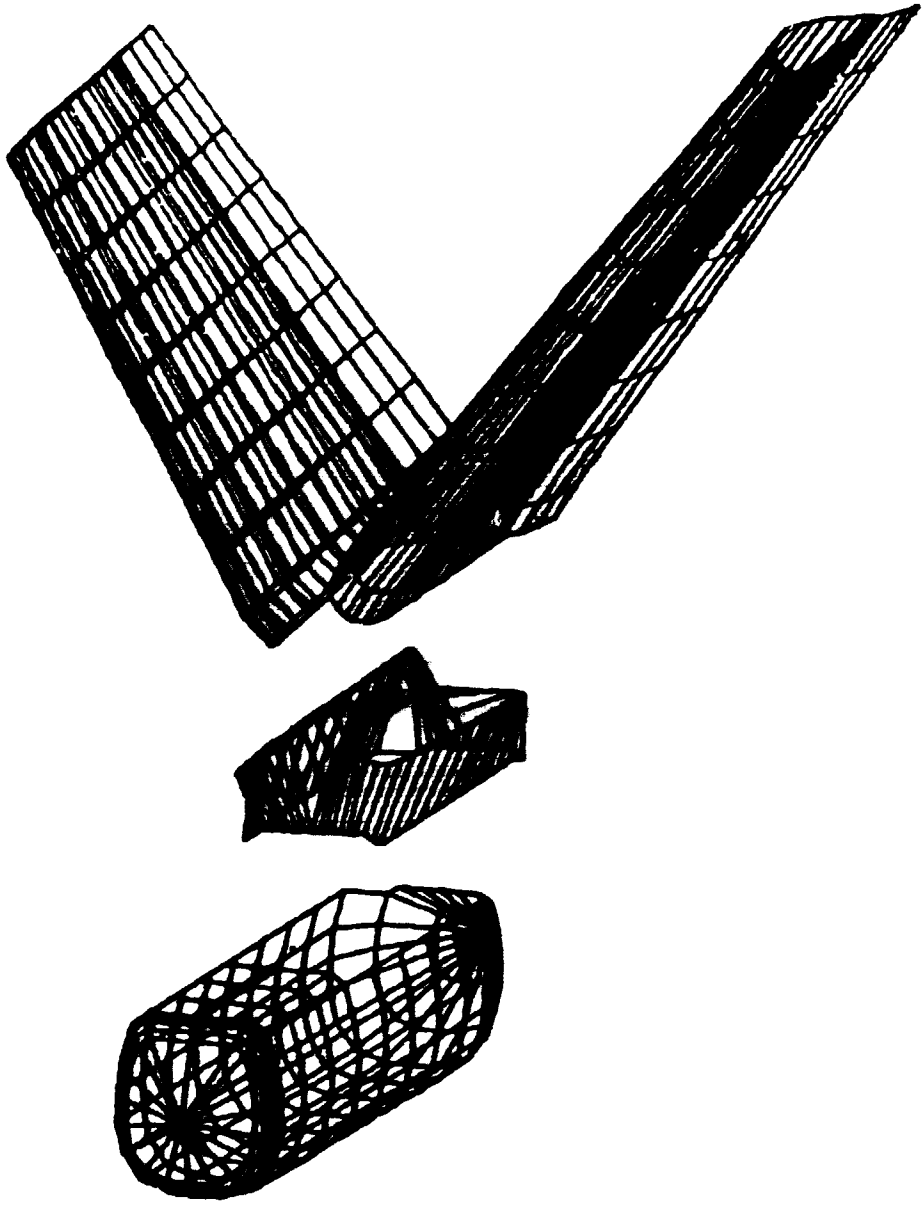

Figure 3.- V-tail paneling geometry.

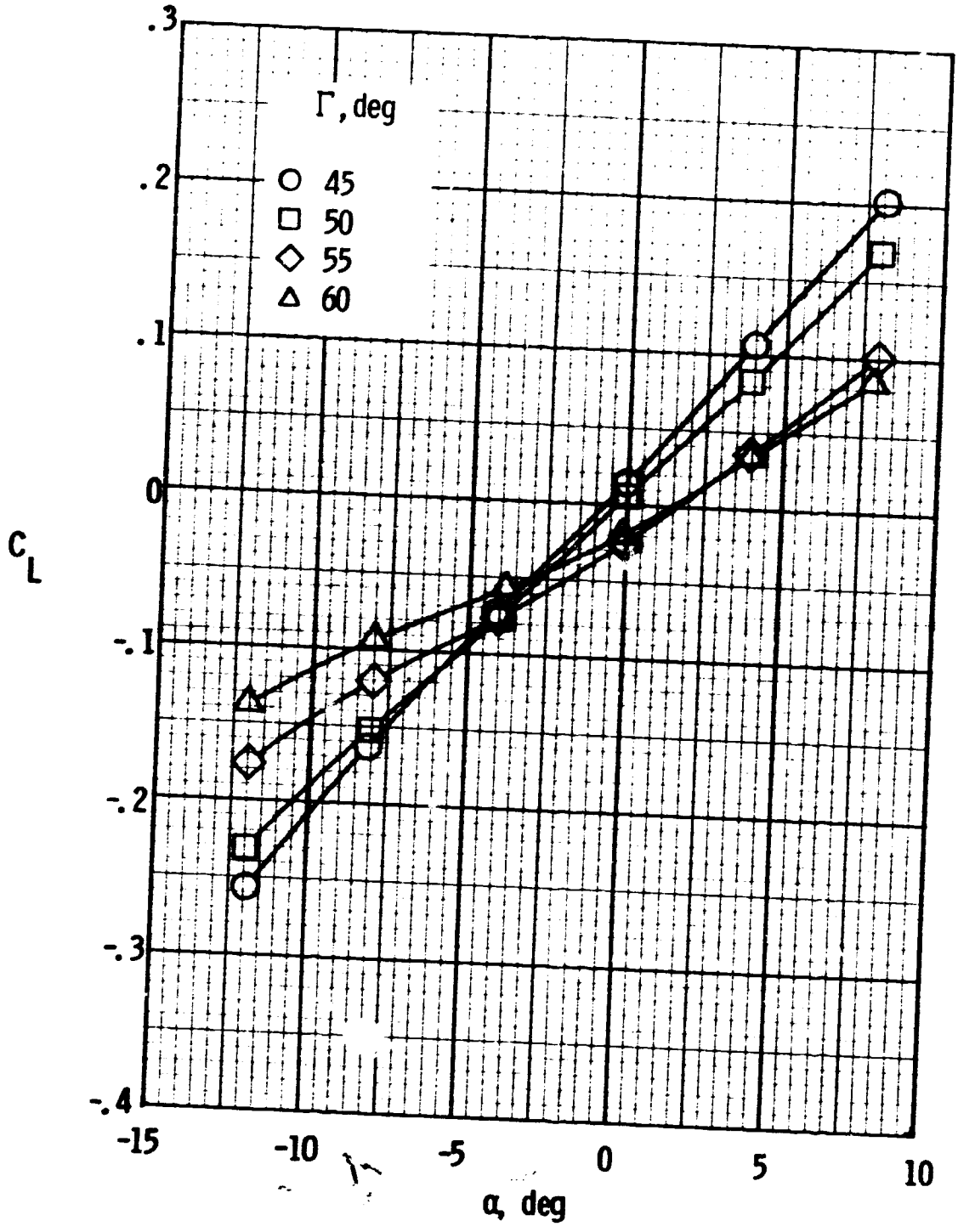

Figure 4.- Effect of dihedral on V-tail lift coefficient.

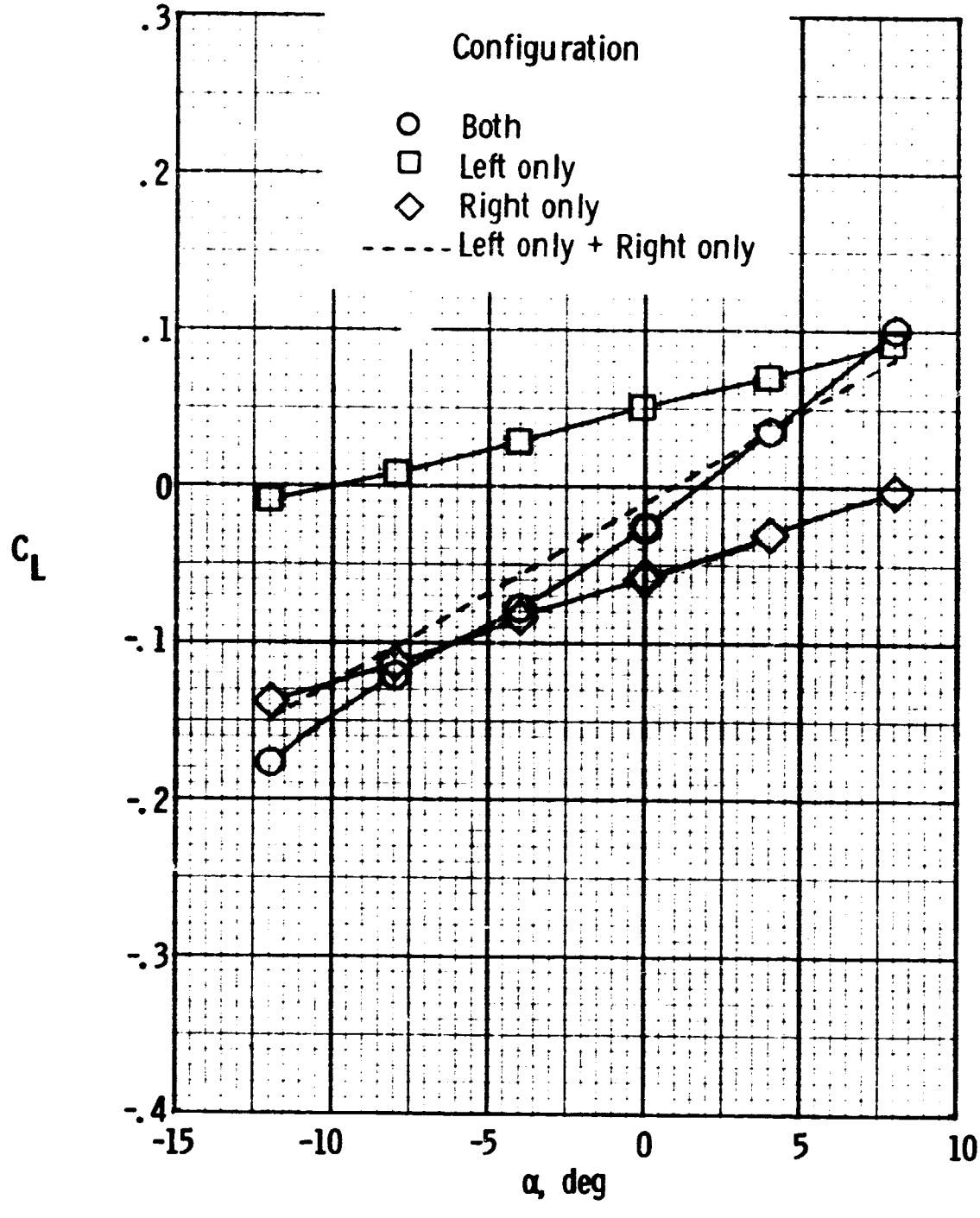

Figure 5.- Comparison of lift coefficient for the V-tail at 55° dihedral and left and right surfaces alone at 55° dihedral.

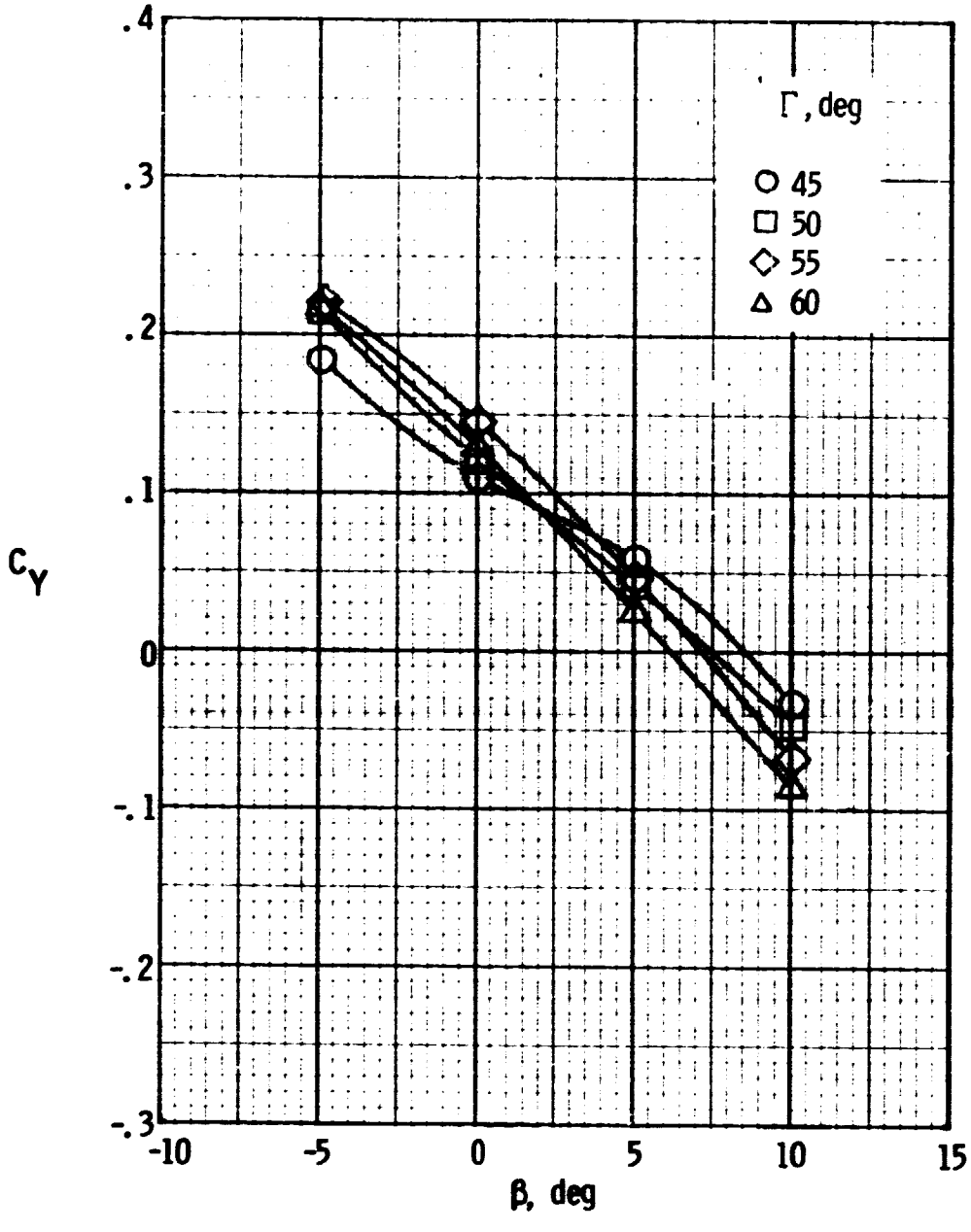

(a) $\alpha = 4^{\circ}$.

Figure 6.- Effect of dihedral on V-tail side-force coefficient.

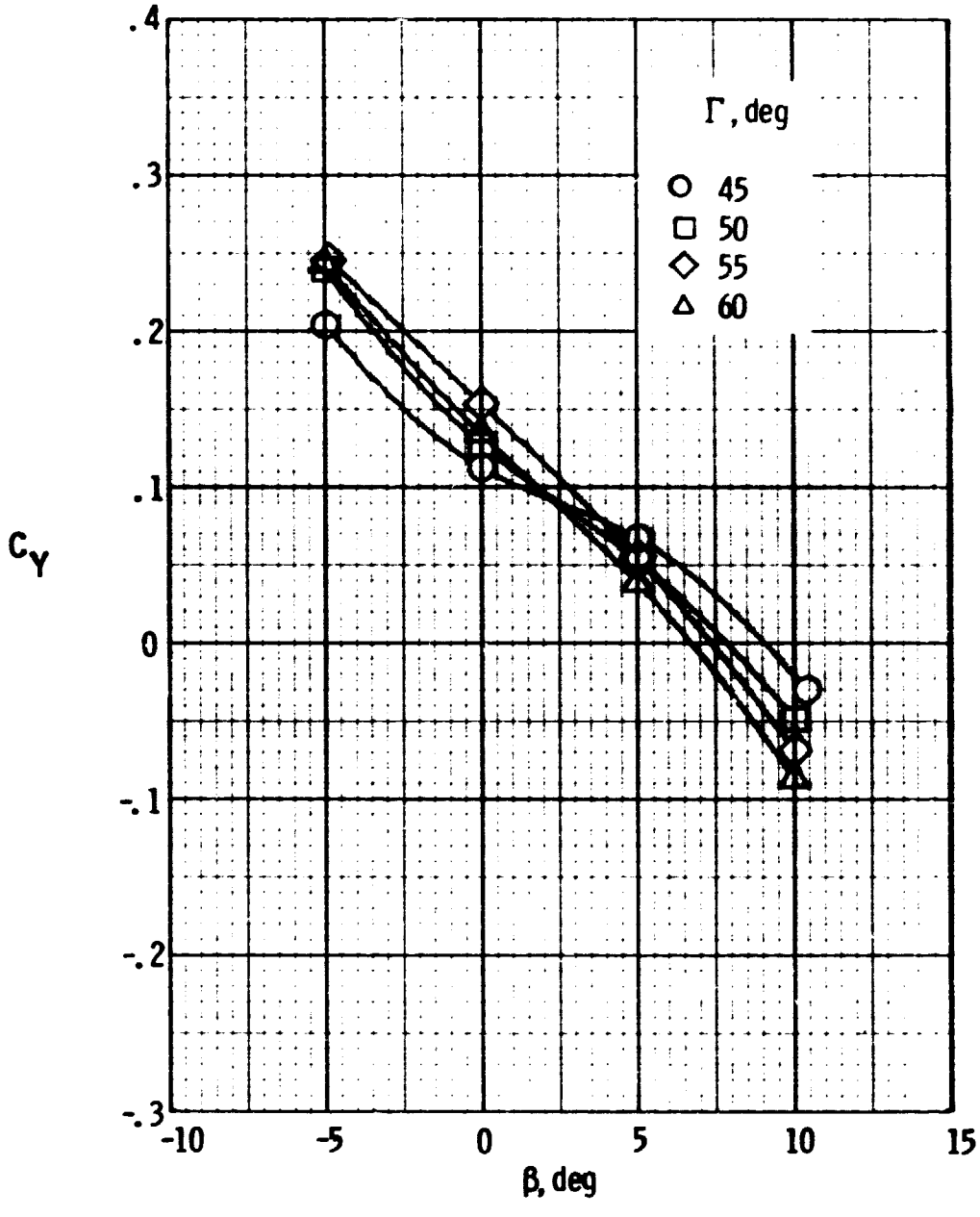

(b) $\alpha = 0^{\circ}$.

Figure 6.- Continued.

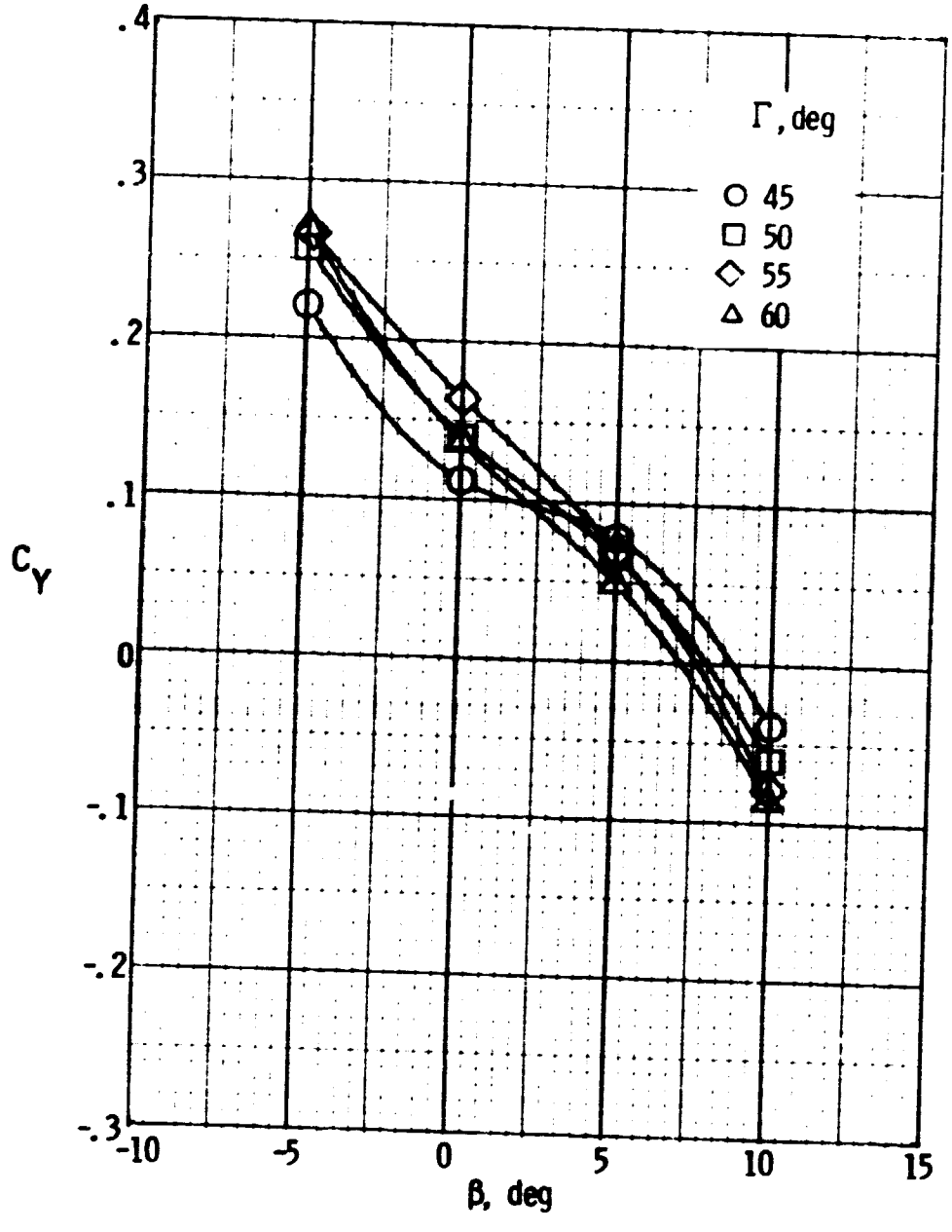

(c) $\alpha = -4^{\circ}$.

Figure 6.- Concluded.

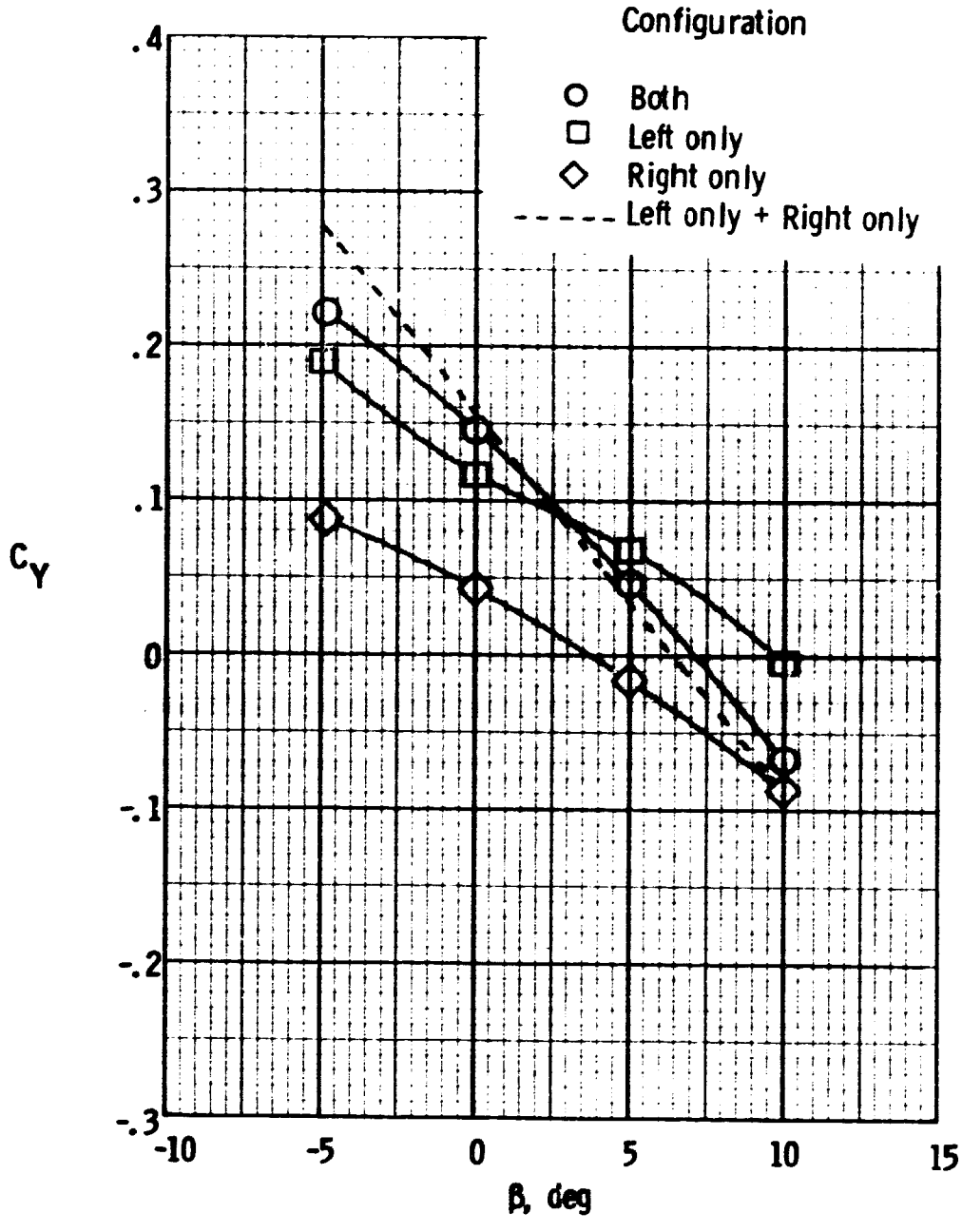

(a) $\alpha = 4^{\circ}$.

Figure 7.- Comparison of side-force coefficient for the V-tail at 55° dihedral and left and right surfaces alone at 55° dihedral.

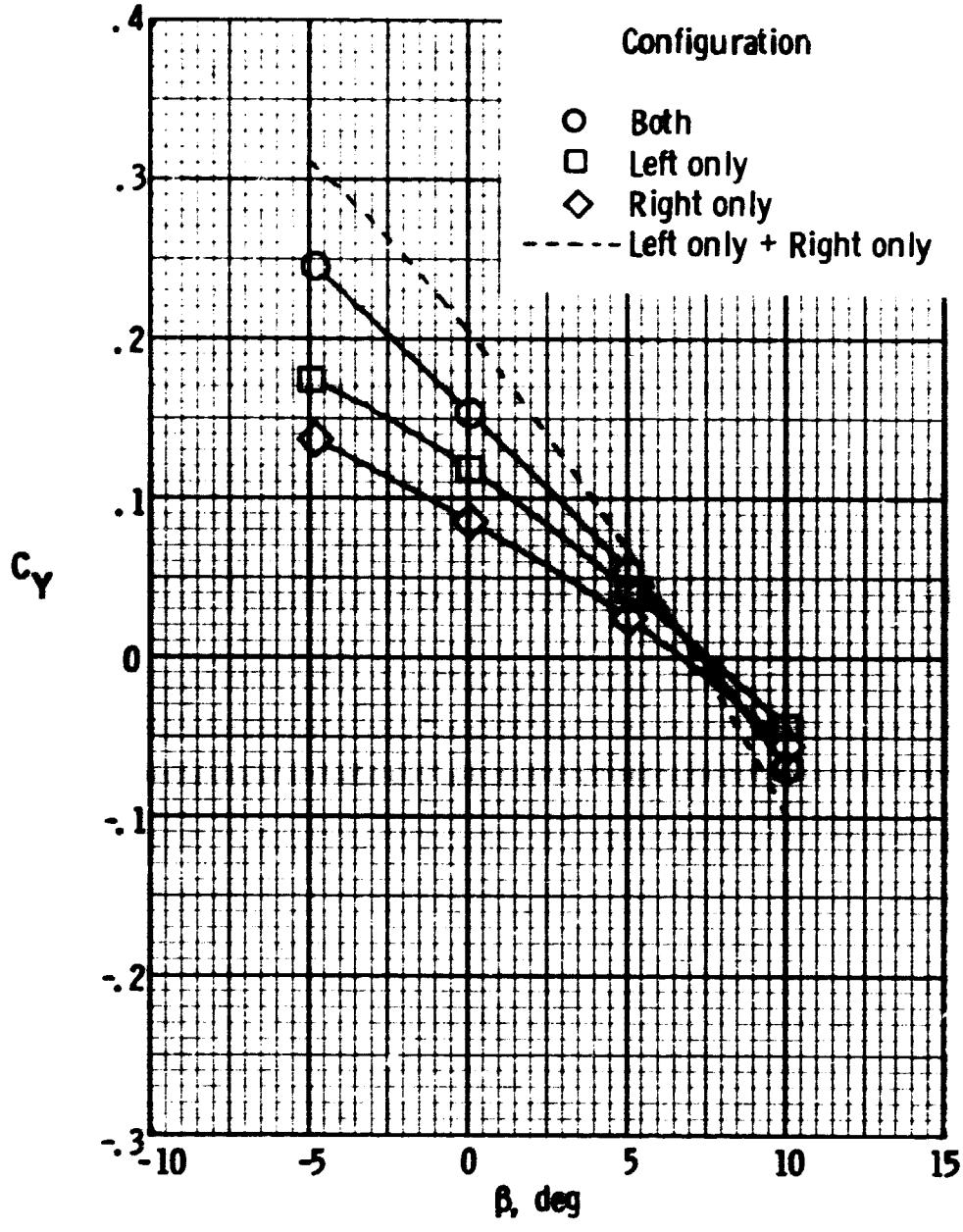

(b) $\alpha = 0^{\circ}$.

Figure 7.- Continued.

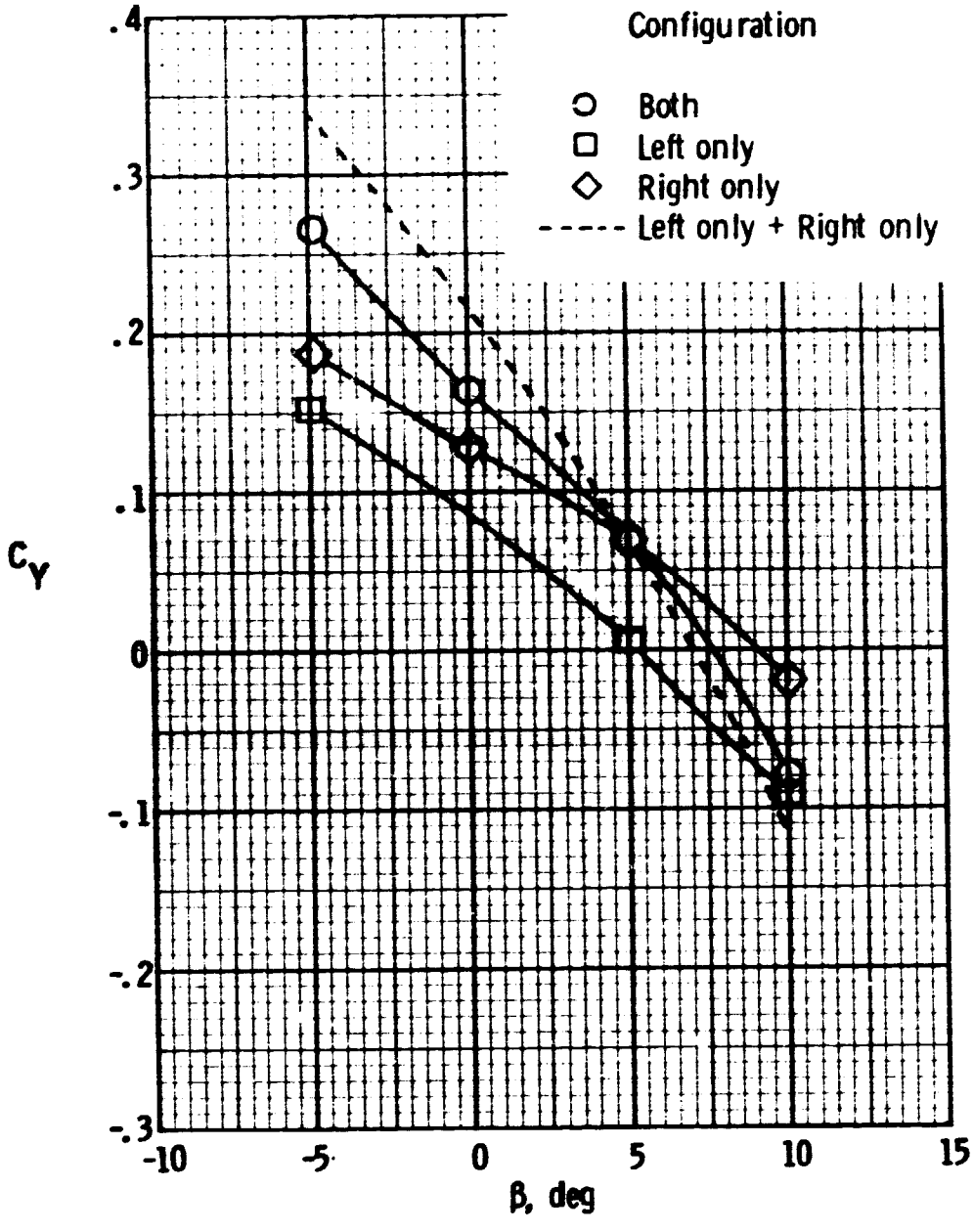

(c) $\alpha = -4°$.

Figure 7.- Concluded.

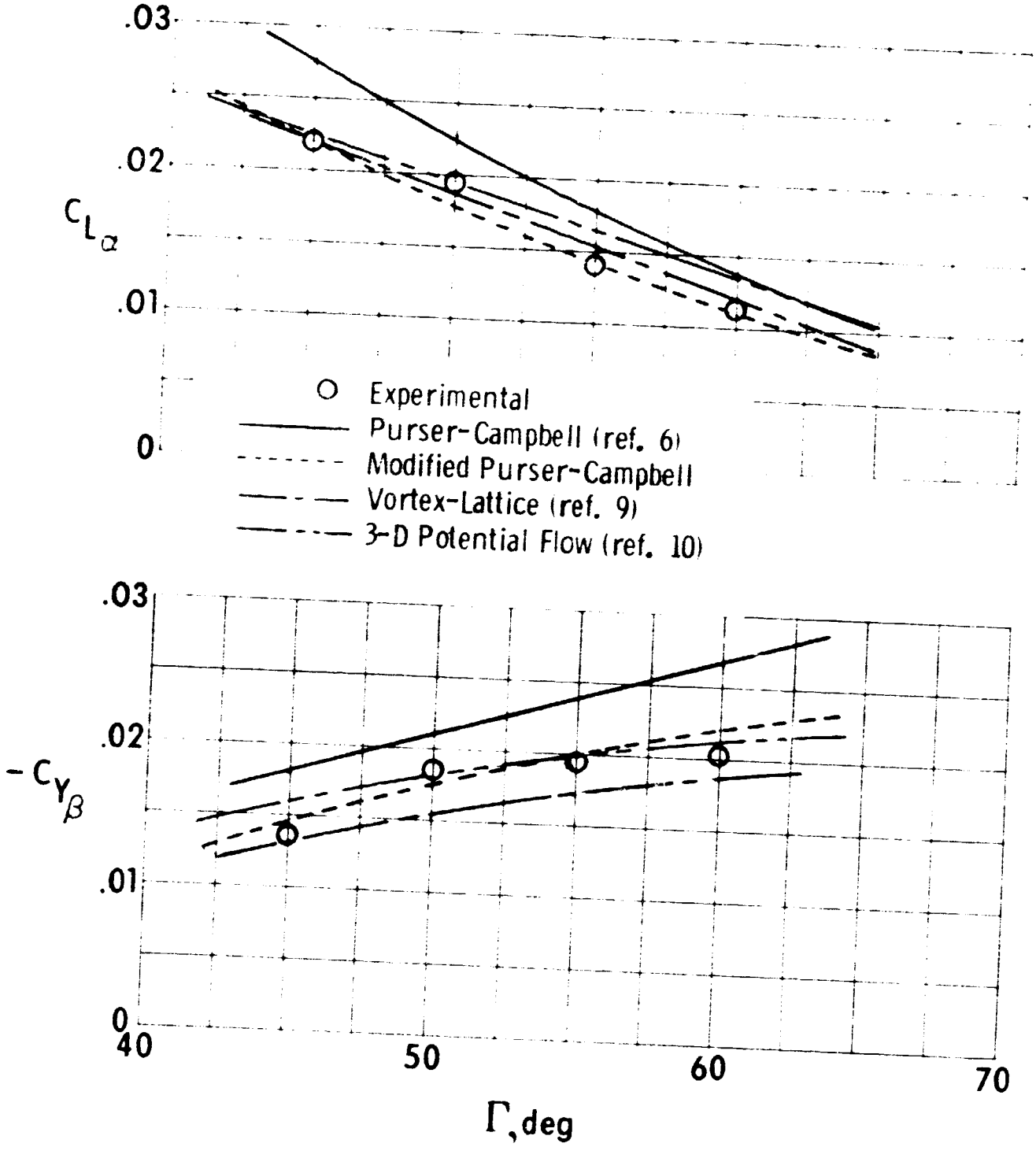

Figure 8.- Comparison of experimentally determined V-tail C_{L_α} and $-C_{Y_\beta}$ with values predicted by four analytical methods.

END

DATE

FILMED

NOV 6 1978